Bioprinting xxx (xxxx) xxx

Contents lists available at ScienceDirect

Bioprinting

journal homepage: www.elsevier.com/locate/bprint

Cost-effective microvalve-assisted bioprinter for tissue engineering

Nami Okubo [a,b,**], A.J. Qureshi [c], Kenny Dalgarno [d], Kheng L. Goh [a], Suchitra Derebail [b,*]

[a] Newcastle University International Singapore, Faculty of Science, Agriculture and Engineering, Singapore
[b] Republic Polytechnic, School of Applied Science, Singapore
[c] University of Alberta, Department of Mechanical Engineering, Canada
[d] Newcastle University, School of Engineering, Newcastle Upon Tyne, United Kingdom

ARTICLE INFO

Keywords:
Bioprinting
Microvalve
Magnetic mixer
Cancer cells
Stem cells
Primary cells

ABSTRACT

There are numerous commercial bioprinters based on the most prevalent bioprinting method of extrusion. Despite the popularity of these bioprinters, other technologies like droplet-based or drop-on-demand systems are rapidly gaining traction. These alternate methods exhibit advantages in terms of cost, reliability and adaptability to a broader spectrum of cell types. This paper describes the development and validation of a cost-effective, droplet-based, microvalve assisted bioprinter. The mean and the coefficient of variation values are reported for cell numbers dispensed *via* three modes: manual pipetting (mode 1), bioprinting without the aid of a cell mixer (mode 2) and bioprinting with the aid of a cell mixer (mode 3). Consistent and reproducible results were obtained when cells were dispensed with a mixer maintaining the cells in a homogenous suspension. The printer was assessed for positional accuracy, variability in cell numbers and post-print viability for a range of cell types. This report demonstrates that it is feasible to custom design a cost effective, microvalve based printer to suit specific cell types for a range of tissue engineering applications.

1. Introduction

In this study, an open-source 3D printer was adapted to create a microvalve-assisted bioprinter (MAB) that incorporated low-cost, readily available hardware, software and control elements, that was evaluated for various parameters. Biofabrication or bioprinting is an emerging, disruptive technology with a broad spectrum of applications in the field of tissue engineering, regenerative medicine and drug toxicology. In its simplest form, this technology involves the accurate and uniform dispensation of living cells suspended in a culture media, into cell culture dishes. In complex workflows, growth factors, multiple cell types, biocompatible bio inks, etc. are used to seed cells onto and into pre-fabricated tissue scaffolds, to produce complex *in vitro* tissues [1–5]. Progress in this field is being driven by an insatiable demand for transplantable tissues and organs; while the waiting list for organs grows each year, the numbers of donors and successful transplants show less dramatic changes [6]. There is also a need for alternatives to animal models in drug toxicology and cosmetic testing. In general, bioprinting needs fall into two broad categories; requirement of complex tissues with either structural or functional value, like multi-layered skin or vascular grafts/bone grafts, and the requirement for tissue models as a testing ground for drugs, toxins, cosmetics etc. [7,8]. Many research studies have shown successful dispensation of cell types with therapeutic value, using different types of print heads, for example, inkjet, laser, syringe or microvalve [9–11]. With the aid of stem cells, this technology is being extended to the creation of more complex organs like brain, bone, trachea, vasculature of tissues, organ chips like lung-on-a-chip etc [7]. There are also a number of commercial printers available that allow the printing of complex cell/material assemblies [9,12].

Despite the rapid progress in bioprinting in recent years, there are numerous challenges [12] that should be addressed to harness the benefits of this technology more effectively. Various modes of bioprinting may stress cells in many ways, for example; shear stress in extrusion, resulting in loss of cell viability, reduced pluripotency or differentiation potential in stem cells, or uncontrolled differentiation into non-specific cell types. If the primary aim is cell dispensing, then, ideally, bioprinting should be achieved in a scaffold-free manner [10,13]. Scaffoldless bioprinting is useful in many applications, including high throughput generation of cell based models, micro-tissues or cell spheroids within culture plates. Such clusters of cells are self-forming and do not require scaffolds to hold their shape post printing. Aseptic techniques are crucial when working with cell cultures; hence it is necessary for all

* Corresponding author.
** Corresponding author. Newcastle University International Singapore, Faculty of Science, Agriculture and Engineering, Singapore.
E-mail address: suchitra_derebail@rp.edu.sg (S. Derebail).

https://doi.org/10.1016/j.bprint.2019.e00043
Received 23 July 2018; Received in revised form 31 December 2018; Accepted 28 January 2019

the surfaces and moving parts that are directly in contact with cells to be autoclavable or to be of cell-culture grade. Cells tend to aggregate during the printing process and cause clogging of the extrusion head. Methods are needed to ensure that cells are constantly in suspension before and during bioprinting, to ensure uniform and highly accurate dispensation of cells. The deposition of cells should be a fast, controllable and highly reproducible process in order to prevent dehydration of cell droplets and subsequent loss of viability and impairment of cell functions. Printing processes should be amenable to automation, and high throughput dispensation. Moreover, it should be cost-effective, to allow more researchers to access this technology to drive cell-based research. The challenges faced in bioprinting have been addressed in many ways by various reports [14,15]. Reid *et al.* have reported using microextrusion [14], in which a low-cost 3D printer was modified and pulled glass microcapillary pipettes were successfully used to print human induced pluripotent stem cells (hiPSCs). The modified printer and needle showed reduction in cell clogging and improved cell resolution and viability. A nozzle-less method was adopted in another report that eliminated the entire concern of clogging and shear stress [16]. The authors demonstrated that this method could be used with a wide variety of cell like hepatocytes, cardiomyocytes and fibroblasts while retaining high cell viabilities.

The quality of printed cells depends on the choice of printhead; information gleaned from multiple reviews of printheads has been collated in Table 1. After weighing the pros and cons of these methods and when viewed in terms of cost effectiveness and cell viability, microvalve based systems were considered the most promising for cell dispensing. Microvalve-based bioprinting is classified as drop-on-demand (DOD) printing, along with inkjet and laser-based bioprinting [3,9,17,18]. In this method, in contrast to the continuous printing, droplets containing cells or other biomaterials are printed out in a controllable, precise manner. A standard microvalve printhead consists of a source for pneumatic pressure, plunger and a solenoid coil. The solenoid coil works like a magnetically actuated micro pump; it consists of a chamber with inlet and outlet valves, a permanent magnet, a flexible membrane and a set of drive coils that provide a controlled magnetic field. By changing the electric current flow through the coil, the strength of the magnet can be changed. This creates an attraction or repulsion movement between the permanent magnet and coils, and this delivers the actuation force necessary to move the plunger in an upward motion. The ascending motion of the plunger aids in the controlled opening of a dispensing nozzle. Multiple nozzles can be attached to the system, with each one having a specific process. This printhead is able to accurately dispense specific volumes ranging from tens of nanolitres (nl) to several microliters (μl). Some of the touted advantages of this system compared to other methods are; high cell viability (>86%) [18], uniform cell dispensation [19], and high throughput printing. This report indicates that microvalves could potentially be used on other cell types that have therapeutic value.

In this study, a cost-effective microvalve-assisted bioprinter (MAB) was designed and then it's performance evaluated using an array of six different cell types. All the cell types were chosen for their value in regenerative medicine, cancer studies and drug testing. These cells were tested in a scaffold-free, bio-ink free mode by suspending them in appropriate culture media prior to dispensation. The post-print cell data reflects the effect of the dispensing method alone on cell numbers and viability. For all bioprinting applications, reliability and scalability are key requirements. In this work, the bioprinter was designed to address key bioprinting challenges, like cell clogging, and post print variability in cell numbers, cell viability and recovery, followed by assessment of the performance and reliability of the MAB in high throughput applications.

Table 1
Comparison of available cell dispensing printheads.

Print head	Advantages	Disadvantages	References
Laser	• No issues of biomaterial clogging and viscosity • High cell viability • High resolution, droplet diameter is 10–120 μm	• High cost • Potential genetic damage to cells • Requirement for laser absorbing material	[9,17,18, 20–24]
Inkjet	• Affordable cost • Usage of multiple nozzles • Continuous or droplet dispensing capability • Moderate cell viability • Moderate to high resolution, droplet diameter is 50–300 μm • Adaptable to high-throughput	• Shear stress applied to cells • Adverse effects of high vibration frequencies and/or thermal effects • Nozzle clogging • Limited size of droplets	[9,17,18, 22,23]
Valve	• Most advantages similar to inkjet method • Low to moderate resolution, droplet diameter is 10 μm – 1 mm • Voltage controllable valve • Low shear stress • Uniform cell dispensation • Gentle on cells, high cell viability	• Nozzle clogging • Droplet size is limited by nozzle size	[9,17,18, 23]

2. Materials and methods

2.1. Machine design

The specifications for the MAB system are shown in Table 2, and the machine setup is shown in Fig. 1. The development of the system was focused on the driving mechanism, micro valve, mixing mechanism and syringe pump.

A RepRapPro Ormerod 2 3D Printer, originally intended for extruding different types of plastics, was modified to dispense droplets of culture media containing cells into a 96-well format cell culture dish (Fig. 1). Only the X, Y and Z controls were used in this design. The extruder was replaced with a VHS Nanolitre Dispense Valve (Lee Products Ltd, INKX0514850A) with a Hex MINSTAC with Jewelled Orifice Dispensing Nozzle - 100 μm (Lee Products Ltd, INZA4650935K). A syringe pump was fabricated using a disposable glass syringe with a 10 ml Luer Lock tip (Thermo Fisher Scientific), a Nema 23 Stepper Motor, and with 3D printed Acrylonitrile Butadiene Styrene frame components constructed using a Makerbot 3D printer. A silicone tube of inner diameter 3.5 mm was used to connect the glass syringe to a 062 to 125/156 Minstac adaptor (Lee Products Ltd, TMDA9502950Z), which in turn connected to a PVC tube of inner diameter 1.05 mm (Lee Products Ltd, TUVA4220900A) which led to the microvalve. To maintain a homogenous suspension of cells during the printing process and to prevent cell clogging in the nozzle, a magnetic mixing system (ThermoFisher Scientific, 88880007) was added to the bioprinter module. Additionally, aluminium frames and wooden blocks were constructed to support the syringe pump above the magnetic stirring mechanism. Positioning jigs made of machined acrylic were used to position a 96 microwell plate in place for accurate dispensation.

Table 2
The microvalve-assisted bioprinter (MAB) system specifications.

No.	Specifications
1	Dispense therapeutic cells with high viability
2	Dispense cells in media with droplet volume of 100 μl–110 μl
3	Positioning accuracy to be more than 85%
4	Dispense into a 96-well plate
5	Have a deposition rate of less than 10 min per 96-well plate

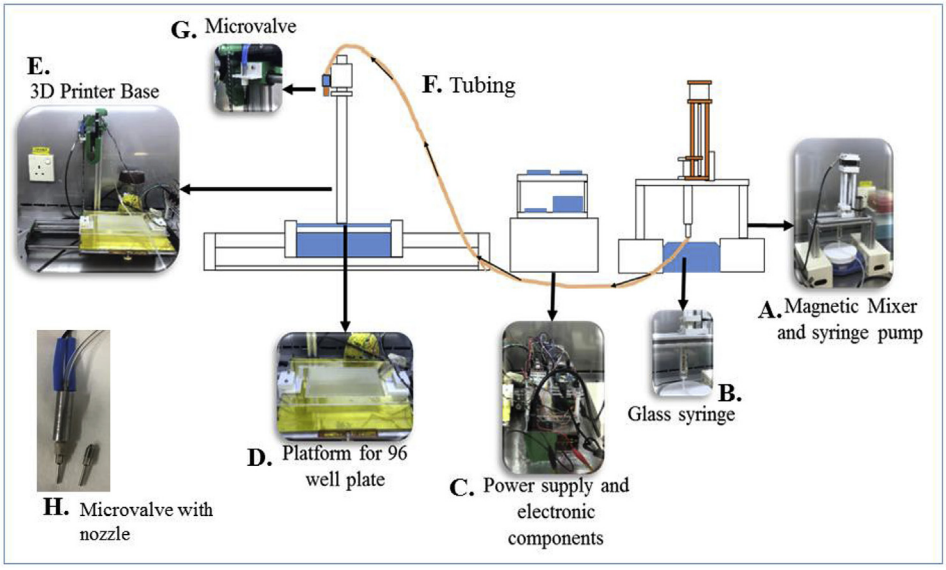

Fig. 1. Schematic diagram of the Microvalve-based bioprinter or MAB: Component parts are labelled from A – H. The arrows on F indicate the direction of sample flow from B to G. Nozzle of 100 μm size (H) was attached to G for testing.

An Arduino Mega board was programmed and used to control the axis motor and syringe pump. The Arduino Mega sent signals to Easy Drivers that allowed the control of the speed and revolution of the motors. It also sent signals to the microvalve driver (Lee Products Ltd, IECX0501350A) to control the opening and closing mechanism of the valve. The microvalve required spike and hold voltages of 24 V and 3.5 V respectively, supplied by a step-up voltage regulator from Polulu for the former and the power supply for the latter. The bioprinter head was designed to move from home position to the initial start position before cell dispensation. It was programmed to sequentially dispense 100 μl into each well, row by row across the 12 rows of the 96-well plates.

2.2. Positioning accuracy

The positioning accuracy was assessed by programming a predetermined distance (referred to as the theoretical distance) for the print head to move based on revolutions of the rotor, and comparing this with the actual distance moved (referred to as the experimental distance), which was measured by a Vernier calliper. The measured distance was correlated to the number of revolutions turned. This experiment was repeated in sets of 10 for 3 different revolutions of the motor, namely; 1, 2 and 3 revolutions.

2.3. Volumetric consistency tests

The incremental weights of distilled water with a nominal volume of 100 μl dispensed either manually or using the bioprinter into a 96-well plate, were recorded. For the manual method, a 200 μl single channel pipette set to a volume of 100 μl, was used. In the bioprinted method, nominal 100 μl volumes were dispensed from a 100 μm nozzle. The recorded weights data were then converted to an average droplet volume (in μl) by dividing the total mass of dispensed droplets (g) by the number of dispensed droplets.

2.4. Cell culture

All cell types used in this experiment were cultured in a laboratory incubator at 37.0 °C (±0.5 °C) and 5.0% CO_2 (±0.5%). All cell types were thawed, subcultured, maintained and cryopreserved as per each manufacturer's instructions. Cells were passaged every 2–3 days with 0.025% trypsin/ethylene diamin tetraacetate (EDTA; PAN Biotech P10-029100) and cells were harvested in the log phase of cell growth for bioprinting experiments. The complete media for each cell type was filtered in 0.2 μm filter, aliquoted into 50-ml tubes and stored at 4 °C. The details for each cell type are shown in Table 3.

2.5. Cell viability and cell recovery assays

All culture experiments were repeated three times to ensure consistency and reproducibility. During routine cell passaging and to quantify the viable cell numbers in cell suspensions prior to dispensation, cells were treated with 0.4% Trypan blue stain solution (Gibco, 15250–061) to evaluate cell viability *via* the exclusion dye test method. Viable cell numbers were determined manually using a hemoctyometer counting device (Heinz Herenz, 1080305). For quantitative assessment of viable cells that were recovered after high throughput dispensation by manual pipetting or by bioprinting, CellTiter-Blue® Cell Viability Assay from Promega (G8081) was used as per manufacturer's instructions. In general, 20 μl of resazurin reagent was aliquoted into each 100 μl of medium containing cells in a 96-well format. Fluorescence values for cell samples were detected using filter sets; 560 nm for excitation and 590 nm for fluorescence emission using Tecan plate reader (Tecan Trading AG Infinite® 200 PRO NanoQuant Plate Reader). The post-print viable cell numbers were compared with viable cell numbers prior to dispensation and are reported here as average cells recovered per well, and as variations in cell numbers across all the 96 wells in a single plate or COV.

For visual, qualitative assessment of both live and dead cells, cells were stained with Calcein AM (Cayman Chemical Company 14948) which is a non-fluorescent, hydrophobic compound that can permeate living cells. 2 mM stock solution was used at a final concentration of 1 μm. Propidium iodide (PI) is a red fluorescent stain that cannot permeate living cells. Stock concentration of 1.5 mM of PI was diluted to 2 μM working solution before staining of all cell types. Post-staining, cells were incubated in the dark for 15–20 min. Fluorescence intensity was recorded using a 490-nm excitation filter and a 520-emission filter for the calcein stain, and an excitation maximum of 535 nm and an emission maximum of 617 nm for the PI stain. Cell images were captured and recorded using an Olympus inverted fluorescent microscope system (1XT3). Three random fields were checked for each sample. Calcein AM and PI stains were used to generate live/dead fluorescent cell images for all the cell types that were dispensed either by manual pipetting or by bioprinting methods.

Table 3
Cell culture specifications.

Cell cultures	Basal cell culture media	Culture supplements
Human Colorectal Cancer cell lines (HCT116) (ATCC® CCL247™)	DMEM or Dulbecco's Modified Eagle's medium/High Glucose (GE Healthcare Life Sciences SH30022.01)	Each 500- ml bottle of basal media was supplemented with 10% FBS or fetal bovine serum (v/v), triple 0.1 μm sterile filtered and heat inactivated (Serana Australia S—FBS-AU-015) 0.1 mM MEM NEA or minimum essential medium nonessential amino acids (PAN Biotech P08-32100), 2 mM L-Glutamine (HyClone® SH30034.01), 100 UmL−1 penicillin/ streptomycin (HyClone® SV30010)
Mouse Embryonic Stem cells (mESCs) from strain C57BL/6 mouse blastocyst (ATCC® SCRC1002™)	DMEM/High Glucose (GE Healthcare Life Sciences SH30022.01). Mouse Embryonic Stem cells (mESCs) were cultured on 35 mm dishes that were pre-coated with 0.1% gelatin dissolved in ultrapure water (Merck Millipore ES-006-B). After every passage, cells were seeded onto 0.1% gelatin-coated Petri dishes.	Each 500- ml bottle of basal media was supplemented with 15% of FBS, triple 0.1 μm sterile filtered and heat inactivated (Serana Australia S—FBS-AU-015), 0.1 mM MEM NEA (PAN Biotech P08-32100), 2 mM L-Glutamine (HyClone® SH30034.01), 1 mM sodium pyruvate (Gibco® by Life Technologies 11360–070), 100 UmL−1 penicillin/ streptomycin (HyClone® SV30010), 1000 UmL−1 leukemia inhibitory factor (LIF: ESGRO, ESG1106) and 0.1 mM β-mercaptoethanol (Sigma Aldrich, M3148)
Primary Normal Human Dermal Fibroblast Adult Cells (HDFa cells, C0135C)	Medium 106 (M106500) supplemented with the Low Serum Growth Supplement Kit (LSGS, S003K) prior to use (all supplied by ThermoFisher Scientific)	Each 500- ml bottle of basal media was supplemented with LSGS kit which has 2% FBS v/v, hydrocortisone 1 μg/ml, hEGF or human epidermal growth factor 10 ng/ml, hFGF or human fibroblast growth factor 3 ng/ml and heparin, 10 μg/ml.
Primary Normal Human Epidermal Keratinocyte cells (NHEKa cells, C-12003)	Keratinocyte growth medium 2 (C20211) which is a serum-free medium that is supplemented with Keratinocyte growth medium 2 kit (C20111, all supplied by Promocell).	Each 500-ml bottle of basal media was supplemented with BPE or bovine pituitary extract 0.004 ml/ml, hEGF (recombinant human) 0.125 ng/ml, insulin (recombinant human) 5 μg/ml, hydrocortisone 0.33 μg/ml, epinephrine 0.39 μg/ml, transferrin, (human) 10 μg/ml and $CaCl_2$ 0.06 mM.
Human bone-marrow derived Mesenchymal Stem Cells (hMSC, ATCC® PCS-500-041™)	DMEM/High Glucose (GE Healthcare Life Sciences SH30022.01)	Each 500- ml bottle of basal media was supplemented with 10% of FBS (v/v), triple 0.1 μm sterile filtered and heat inactivated (Serana Australia, S—FBS-AU-015), 0.1 mM MEM NEA (PAN Biotech P08-32100), 2 mM L-Glutamine (HyClone® SH30034.01), and 100 UmL−1 penicillin/ streptomycin (HyClone® SV30010).
Human umbilical vein endothelial cells (HUVEC cells, CC-2517, single donor)	Endothelial Basal Medium-2 (EBM™-2, CC-3156) supplemented of with EGM™-2 SingleQuots™ (CC-3162, all supplied by Lonza).	Each 500- ml bottle of basal media was supplemented with hEGF, 0.5 ml, VEGF or vascular endothelial growth factor, 0.5 ml, R^3-IGF-1 or recombinant analogue of human insulin-like growth factor, 0.5 ml, ascorbic acid, 0.5 ml, hydrocortisone, 0.2 ml, hFGF-β, 2.0 ml, heparin 0.5 ml, FBS, 10.0 ml, and GA or Gentamicin/Amphotericin-B, 0.5 ml.

2.6. Standard curves and cell dispensation modes

To generate standard curves for each cell type, viable cell numbers for each cell type was determined using 0.4% Trypan blue stain solution and manual counting of unstained cells, prior to dispensation. Then viable cell suspensions of nominal numbers of 10^5 cells/ml were dispensed into 96-well plates using 3 different increment values; 2 μl, 5 μl and 10 μl per row. After addition of resazurin, plates were incubated and readings were recorded at 4 h post-incubation, using the Tecan plate reader, and standard curves generated from the data.

Cell samples were dispensed *via* three modes, namely manual (mode 1), bioprinting without mixer (mode 2) and bioprinting with mixer (mode 3). In the mode 1, a 100 μl volume of viable cell suspensions of nominal numbers of 10^5 cells/ml were dispensed into 96-well plates, using a 200 μl single channel micropipette. Single channel was used instead of multichannel, in order to obtain data that is comparable with well-to-well dispensation from a single print head in the bioprinter. In the modes 2 and 3, cell dispensation was done using the same volume and cell numbers as in mode 1, with the aid of a 100 μm nozzle and either with or without a mixer attached to the main body of the bioprinter, respectively.

Then, for each cell type and dispensing method cells were separately dispensed onto 96-well plates. After addition of resazurin and incubation for 4 h, fluorescence data was recorded and cell concentrations estimated using the corresponding standard curve. The coefficient of variation (COV) was calculated from;

$$CV = \frac{\sigma}{\mu}$$

where σ is the standard deviation of the spread of data, and μ is the mean of the spread of data [25].

2.7. Statistical analysis

All cell culture experiments were conducted as triplicates to ensure consistency and reproducibility, as highlighted in previous section. All data were presented as mean ± standard deviation. The statistical significance of experimental data was determined by two-way analysis of variance (ANOVA) [26] to compare values derived for manual and bioprinted methods for each cell type. The paired wise test was evaluated using the Tukey post-hoc test at the significance level of less than 0.05 ($p < 0.05$) available in Graphpad Prism software (version 7.04). Box and whisker plots were obtained for the data generated for all cell types. In the graphical display of the results for each repeat, the error bar indicates the variability of the mean value over 96 wells in a single plate.

3. Results

3.1. Machine positional accuracy

The positional accuracy was greater than 98% in the X and Y axes, respectively and ranges from 81.33% to 89.50% in the Z axis. In Table 4, the averages of each set of 10 for three different rotor revolutions (1–3)

Table 4
Accuracy testing of the three axes (X, Y and Z).

X-axis (number of revolutions	Average theoretical distance (mm)	Average experimental distance (mm)	Percentage accuracy (%)
1	37.70	37.20	98.67
2	75.40	74.59	98.93
3	113.10	111.29	98.40
Y-axis (number of revolutions	Average theoretical distance (mm)	Average experimental distance (mm)	Percentage accuracy (%)
1	37.70	37.37	99.12
2	75.40	75.22	99.76
3	113.10	111.94	98.97
Z-axis (number of revolutions	Average theoretical distance (mm)	Average experimental distance (mm)	Percentage accuracy (%)
1	1	0.87	87.00
2	2	1.79	89.50
3	3	2.44	81.33

are shown for X, Y and Z axes.

3.2. Dispensed volume repeatability

The average volume of nominal 100 µl aliquots of distilled water dispensed into the three 96-well plates was calculated to be 142.08 µl for the manual method as compared to the average volume of 115.22 µl for the bioprinter assisted method, as in Fig. 2. The calculated percentage errors of 42% and 15.2% were obtained for manual and bioprinted methods, respectively. COV values for both methods were calculated, with an average of 0.139 versus 0.089 for the manual and bioprinted methods, respectively.

3.3. Bioprinter evaluation with HCT116 cells

The overall design of the bioprinter, complete with 100 µm nozzle and mixer module was tested by comparing cell counts of HCT116 cell samples dispensed *via* three modes, namely manual (mode 1), bioprinting without mixer (mode 2) and bioprinting with mixer (mode 3). Negative control consisted of HCT116 cells treated with 30% hydrogen peroxide which causes cell death by oxidative stress. The actual numbers of total cells dispensed in each method cannot be gauged accurately, so the evaluation of bioprinter and printing modes was done by comparing

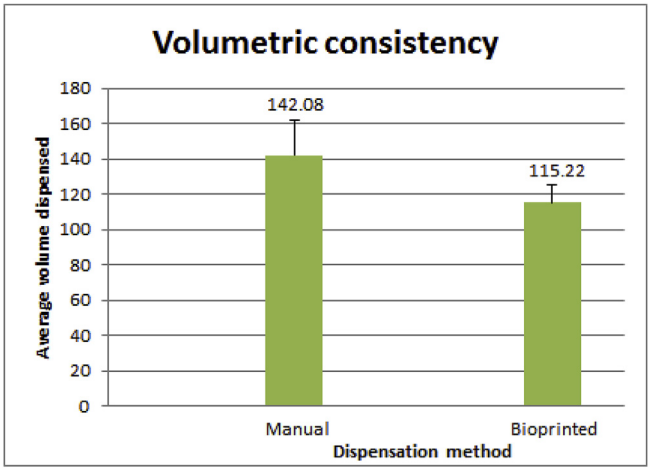

Fig. 2. Volumetric validation of the MAB: Average volumes (in µl) of distilled water dispensed into 96-well plates by manual and bioprinter assisted methods are represented graphically.

post-print, recovered, viable cell numbers with the values prior to dispensation. Approximately, 100 µl of bio-ink (cells suspended in culture media) was dispensed into each well of a 96-well plate and the average numbers of viable cells recovered from each method was estimated to be 159 cells/well for the negative control, 447 cells/well for mode 1 and 635 cells/well and 720 cells/well for the modes 2 and 3, respectively (Fig. 3).

Additionally, variation in dispensed cell numbers for the three modes was estimated after dispensation of a 100 µl volume of culture media (containing nominally 10^5 cells/ml), into each well of a 96-well plate. Data sets were analysed for average cell counts post-printing and variation in cell numbers across the 96-well plate, using two-way ANOVA. Results show a significant difference ($p < 0.0001$) in cell counts or cells/well when mode 1 was compared with the other two modes (Fig. 4, panel A). Average cell numbers post-printing ranged from 730 to 1070 cells/well for each repeat (sets 1–3) of mode 1. Whereas, average cells numbers for mode 2 was higher and ranged from 1230 to 1320 cells/well and for mode 3 it was highest at 1370–1500 cells/well. Data distribution was evaluated using box and whisker plots as shown in Fig. 4, panel A. Box plots for sets 1–3 on mode 1 show longer upper and lower whisker and a wider spread of cell numbers, as compared to modes 2 and 3. In each set, mode 3 shows a tighter distribution of cell numbers, with a majority of data points lying closer to the median values.

With regards to the COV or the cell count relative to the mean (Fig. 4, panel B), for each set, the COV is lower for cells dispensed by mode 3 with an average value of 8.54, as compared to mode 1 and mode 2 with average values of 30.1 and 16.5, respectively. Fig. 4, panel C shows the comparison of average COVs for sets 1–3 dispensed *via* the three modes. COV of mode 3 is significantly different from that of mode 1, as indicated by the p value ($p < 0.000$).

3.4. Bioprinting of different therapeutic cell types

MAB cell dispensation (nominal volume of 100 µl of culture media with cells) using only mode 1 and mode 3 was evaluated for five different cell types: mouse embryonic stem cells (mESC), human mesenchymal stem cells (hMSC), adult human dermal fibroblasts (HDFa), adult normal human epidermal keratinocytes (NHEKa) and human umbilical vein endothelial cells (HUVEC). Fig. 5, panels A–E shows the comparison of cell counts between manual and bioprinted method for every cell type. Apart from a few cases, for instance, set 2 of MSC (p value > 0.999), the majority show a significant difference in cell counts or cells/well for the two methods.

Fig. 6, panel A is an overview of cell count distribution of set 3 for all cell types. All cell types show a tighter distribution of cell numbers for mode 3 as compared to mode 1. Fig. 6, panel B shows the comparison of COV values between mode 1 and 3 for each cell type. With the exception of HDFa cells, all the others showed a substantial decrease in variability of cell numbers for the bioprinted samples.

3.5. Live/dead cell assessment of printed cells

Fig. 7 is a live/dead cell assay for all six cell types tested. It shows cell images taken after manual and bioprinted modes of cell dispensation using the magnetic mixer and 100 µm size nozzle for all the cell types. Calcein AM and propidium iodide reagents were used to indicate live/dead cells as green or red colored cells, respectively. In each case, as shown pictorially, the live/dead cells were comparable between manual and bioprinted modes, indicating that there were no visible adverse effects on bioprinted cells.

4. Discussion

The major design aspects of the MAB described in this paper include; a standard open-source microvalve printhead, a syringe pump, magnetic agitator or mixer, XYZ stage and an electronics board. These

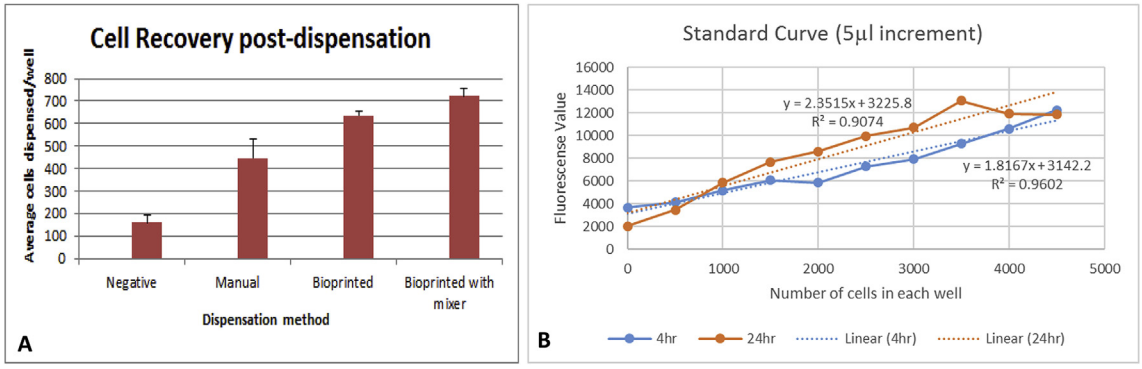

Fig. 3. HCT116 cells were printed manually or by using 100 µm nozzle, with or without mixer. About 100 µl volume of culture media containing cells were dispensed into each well. Panel **A** shows the comparison of average numbers of recovered cells from a 96-well plate, post-dispensation, by different methods. Negative control values are for cells dispensed after treatment with 30% hydrogen peroxide. Panel **B** shows the corresponding standard curve that was used to calculate cell numbers. Readings at 4 h gave a better R^2 value of 0.9602 than the 24 h time point.

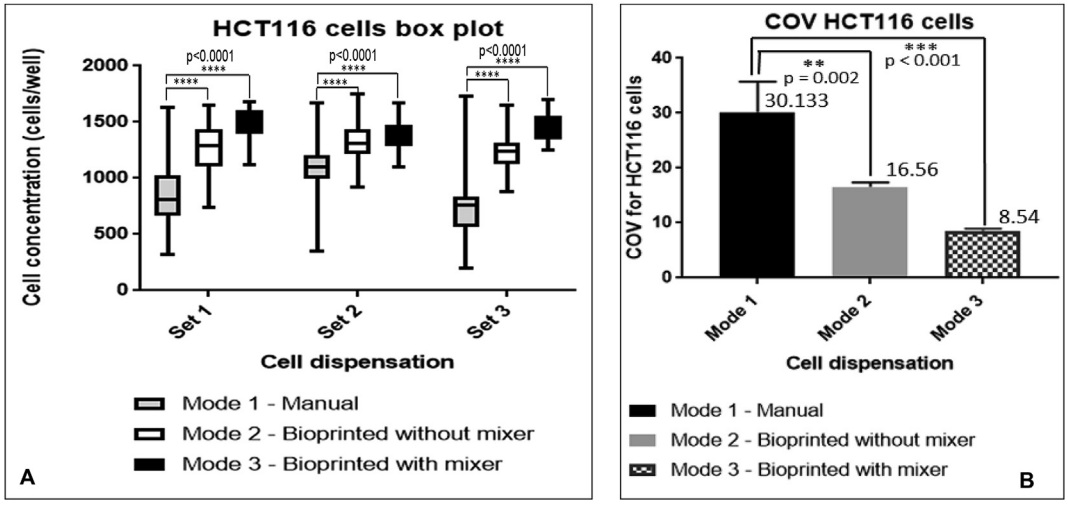

Fig. 4. Panels **A – B** show the comparison of data sets for HCT116 cells, by two-way ANOVA analysis and box and whisker plots **(A)** and COV values **(B)**. Cell counts were determined post-printing using three modes 1–3 as indicated in the figure. Data generated in three experimental repeats are shown as Set 1–3. In Panel **B**, the average COV values for all three sets are shown.

modifications were specifically incorporated into the system, with a focus on some key issues in bioprinting like cell clogging, cell viability, repeatability and consistency in cell numbers post-printing. The printhead was provided with a hold voltage of 3.5 V and a spike voltage of 24 V to avoid damaging the solenoid coil and the printed samples. A syringe pump was used to provide a positive pressure of 8 psi to the plunger within the printhead. A nozzle diameter of 100 µm was used to dispense six different cell types ranging from 10 µm–30 µm in cell diameter. The nozzle was directly mounted onto the microvalve to reduce the overall size of the valve. This caused a reduction in the time taken for the cell suspension to travel from the microvalve until it exits the nozzle. In spite of the multiple advantages of microvalve printing method, the limited range of nozzle size available posed a challenge: cell clogging. This was solved by attaching a magnetic mixer to the syringe pump to keep cells in uniform suspension before and during the printing process. The mixer aided significantly in maintaining the homogeneity of cell suspensions which in turn prevented a build-up of cells at the nozzle's orifice and allowed for a sequential printing into multiple 96-well plates.

The bio printer's design features allowed for all of the system specifications (as listed in Table 2) to be met. Positional accuracy of all three axes was estimated to be quite high (98% for X and Y axes, and up to 89.5% for the Z axis in Table 4). The reason for the poorer accuracy in the z axis is not clear, but we assume that this axis of the RepRap printer was poorly calibrated. However, the errors were repeatable and so once a program had been developed which worked for a 96 wellplate, the program could be executed consistently. The printer was able to accurately dispense 100–110 µl volumes of liquid into each well of a 96-well plate with high accuracy and very low percentage error (15.2%) and COV values (0.089) as compared to manual dispensation (42% and 0.139, respectively) (Fig. 2). The dispensation rate was approximately 4.5 min for one 96-well plate. When the 100 µm nozzle in conjunction with the mixer (mode 3) was used to dispense culture media containing HCT116 cells into 96-well plates, cell recovery values were found to be the highest, with an average of 720 cells/well, as compared to dispensation *via* manual or mixer-free methods (447 and 635 cells/well, respectively; Fig. 3). Mode 3 also showed uniform dispensation of cells across all the wells of the culture plate, for all three repeats of the experiment. Average cell counts for Mode 3 were the highest at 1370–1500 cells/well (Fig. 4, panel A) and closest to the value of the initial cell sample used for dispensation (1000–1500 cells/well). Moreover, when data for cell counts were analysed and compared by two-way ANOVA, box and whisker plots and COV values, it was seen that there is significantly less variation in cell dispensation ($p < 0.0001$), with a majority of data points clustering near the median, and the lowest COV of 8.54 for mode 3. The results were reproducible and consistent across all three repeats, sets 1–3, for HCT116 cells (Fig. 4).

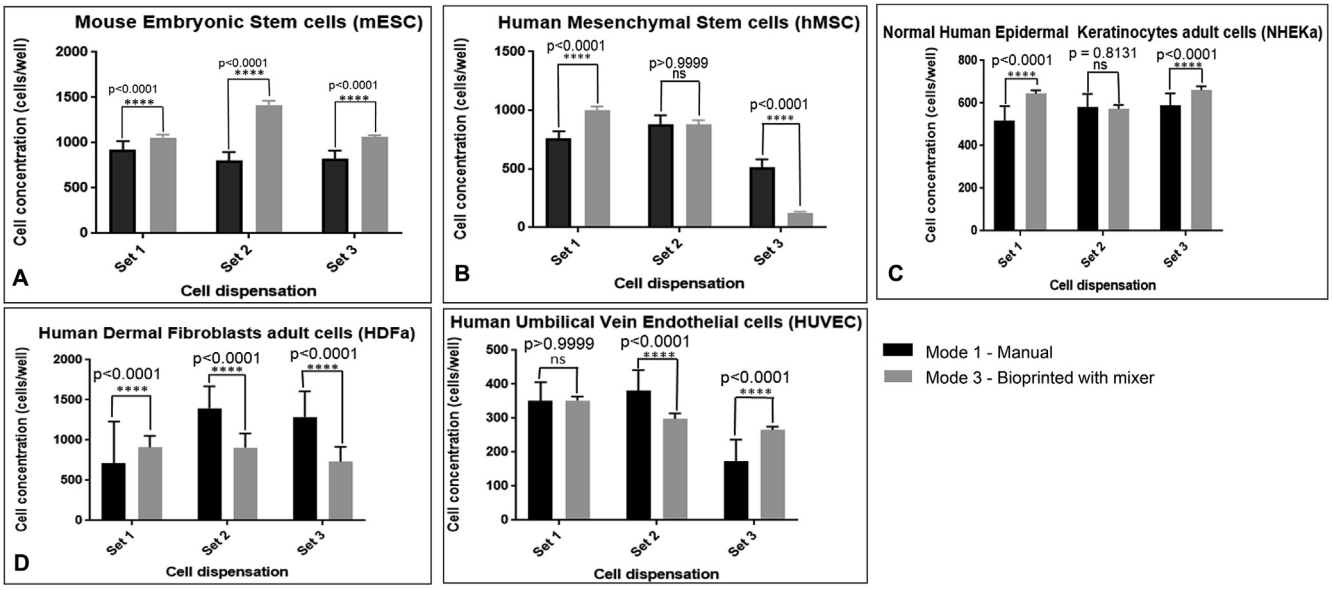

Fig. 5. Panels **A – E** show the comparison of data sets for five different therapeutic cell types as indicated, using two-way ANOVA analyses. Cell counts for 96-well plates were determined post-printing, using two - modes 1 and 3, as indicated in the graph's key. Data generated from three experimental repeats are shown as Set 1–3.

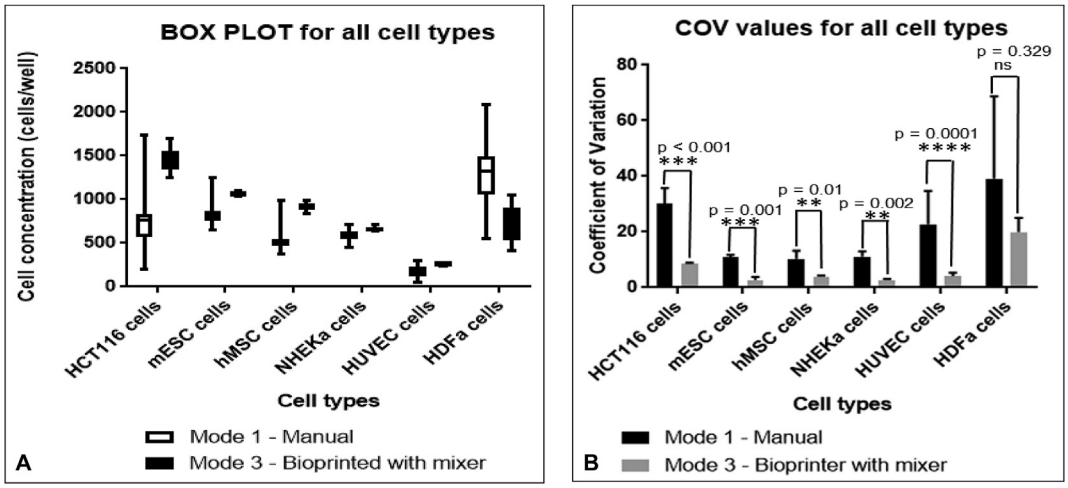

Fig. 6. Panels **A – B** show the comparison of data sets for six different therapeutic cell types as indicated, using box and whisker plots **(A)** and COV values **(B)**. Cell counts were determined post-printing using two modes 1 and 3, as indicated in the graph's key. Data generated from three experimental repeats are shown as Set 1–3.

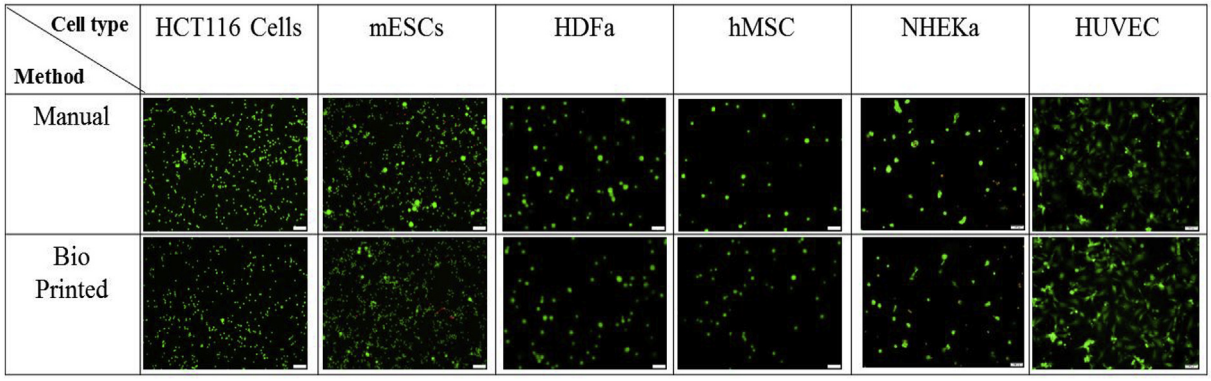

Fig. 7. Live/Dead cell assay: Six cell types were evaluated for viability after printing by manual and bioprinted methods (100 μm with mixer). Calcein and Propidium Iodide (PI) stains were used to stain the cells green (live) and red (dead). Fluorescence intensity of cells was recorded using 490 nm excitation filter and a 520 emission filter for calcein and excitation maximum of 535 nm and an emission maximum of 617 nm for PI stain. The size of the scale bar for all the cell images is 100 μm. (For interpretation of the references to color in this figure legend, the reader is referred to the Web version of this article.)

The bioprinter was further evaluated using five other cell types. Mouse embryonic stem cells (mESC) mirrored all the results seen with HCT116 cells, in terms of cell recovery, uniform cell dispensation etc. For all the other cell types too, consistency in cell deposition and low variation was evident (Figs. 5 and 6). However, there were a few differences in some of the printing parameters; cell recovery values were lower for mode 3 in a few sets (sets 2 and 3 in HDFa), COV was not significantly lower for mode 3 in HDFa cells. Also, for hMSC, NHEKa and HUVEC cells, at least one of the three sets did not show significant difference between manual and bioprinted modes (Fig. 5). These differences in printing are considered to be caused by differences in sizes between the tested cell types. Approximate values for cell diameter are; HDFa/NHEKa – 25–30 μm, MSC/HUVEC – 15–16 μm, HCT116/mESC – 10–12 μm. It is worth noting that changes of ~20% in cell diameter will result in changes of ~50% in cell volume, which are likely to significantly change the behaviour of the bio-ink both in the agitator and in the microvalve. The results suggest that different cell types would need to have their cell concentrations and agitation conditions optimised for maximum yield of deposited cells for a given nozzle size.

Post-printing, live and dead cell assessment was evaluated with the aid of calcein and PI stains (Fig. 7). The results showed that cell mixing using the magnetic mixer and dispensation *via* the solenoid valve did not impose any discernible deleterious effects on the tested cells. Overall, the design features of this MAB provided many benefits that outweighed some of the inconsistencies seen in the printing of different cell types. As all the hardware parts and controls were either sourced from various online vendors or 3D printed and the software program was developed in-house, the overall costs were in the range of $3000 - $4000. The results do show that there is no one-size-fits all design of a bioprinter, and that there is a need to further adapt the MAB to suit specific cell types or applications.

Microvalves are increasingly being employed to print biological materials for many research applications. A commercial version called The Biofactory (regenHu Ltd., Switzerland) was shown to be capable of lung tissue engineering [27]. It was used to achieve layer-by-layer bioprinting of a human air-blood tissue barrier analogue made of endothelial and epithelial cells and a basement membrane. These types of artificial lung models have applications in drug testing and in regulatory toxicology studies [27]. Under non-commercial printers, one example is the printer developed by Faulkner-Jones *et al.* [19,28]. It is the first study that analysed the effect of microvalve printing process on the cell viability and pluripotency of human stem cells (hESCs). Microvalve printing of embryoid bodies (EBs), using hESC, resulted in dramatically smaller size variations when compared with EBs produced manually. Their results indicate that their printer has high spatial accuracy, high speed (40 droplets per second), and high cell viability. The same research group have also successfully used this printing method to generate hepatocyte-like cells from human pluripotent stem cells [28]. It was again demonstrated that the process did not affect the pluripotency of the stem cells and the downstream differentiation process leading to hepatocyte-like cells. Lee *et al.* have shown the biofabrication of fibroblasts containing hydrogel scaffolds with microfluidic channels, which is meant to mimic *in vivo* tissues [29]. Most of these reports show the usage of an array of different cell types of therapeutic value. Additionally, a host of biomaterials are being co-printed along with these cell types [17]. Reagents like alginate, collagen, fibrin, polyetheline glycol, gelatin, biopolymers etc. are routinely used either as bioinks or as scaffolds to support cells during the printing process. Other materials like DNA, drugs, hormones and growth factors are also making their way in biofabrication [30,31]. This indicates that any custom-designed printer would be required to cater to innumerable printing needs and research applications.

While it is not possible to design a universal printer to meet all these demands, we have shown that it is feasible to design a printer that can fulfil at least a subset of these needs. Each of the cells tested on our printer has been shown to have therapeutic value in research or regenerative medicine and we have demonstrated that they can be printed with reliable consistency and cell viability. Keratinocytes and fibroblasts are regularly used by research groups that generate *in vitro* skin either for transplantation or for drug testing [32–34]. Mouse embryonic stem cells and mesenchymal stem cells are used in differentiation studies to generate a range of cell types like cardiomyocytes, neural stem cells etc [35,36]. Endothelial cells are vital for generation of vasculature in bioprinted tissues and organs, as they are capable of *in vitro* angiogenesis [37]. Microvalves do not show a high resolution as compared to inkjet method; ~150 μm vs ~20 μm [18], but the larger volumes deposited are more suited to co-printing multiple biomaterials like cells, specific genes, hydrogels like collagen and alginate, growth factors etc, which requires a bigger nozzle size. Hence there is a trade-off between reduced printing resolutions versus printer productivity and versatility. Future design aspects would require considering the evolving needs of the medical and clinical research industry.

The MAB printer will be further developed to extend its applications in tissue engineering and drug/cosmetic toxicology testing. For example, since the European Commission's issuance of a complete ban on all animal-tested cosmetics and their ingredients, they have been urging their trading partners to follow suit. This has led to a scramble for alternatives to animal testing by a majority of the cosmetic industries. Some proposed solutions include artificial skin constructs for the testing of topical creams. Bioprinters can be used to automate the process of creating homogenous skin sheets to serve as a testing ground for cosmetic ingredients. Another application is in drug toxicology testing and in personalized medicine. Using microvalve bioprinters, human embryonic stem cells can be printed out as droplets of highly uniform cell spheroids or embryoid bodies (EBs) that mimic the developmental processes of embryogenesis. These spheroids consist of ectoderm, mesoderm and endoderm and are representative of all three germ layers of a growing embryo. These EBs have multiple applications; differentiation into different tissue types (cardiac cells, hepatocytes etc.) which can be used in tissue transplantation, development of personalized medicines and embryotoxicity testing. We conclude that this method of cell printing has potential to serve as a platform for a broad array of tissue engineering applications.

5. Conclusion

The fully developed and assembled MAB system (Fig. 1) was validated for various parameters; accuracy of the three axes, volumetric validation, and evaluation of magnetic mixer and nozzle sizes, consistency in printed cell numbers, and cell viability post-printing. The MAB was also tested for its ability to support printing of cells that can be broadly categorized into three cell types; cancer cells, stem cells and primary cells. All cell types were resuspended in appropriate culture media and were printed in scaffold-free and bio-ink free conditions. Most of the results show that the MAB along with the modifications is able to successfully print a wide range of cell types. There were many major benefits noted in the final design of the system; cost effectiveness, high cell recovery, uniform cell dispensation, lack of cell clogging, capability to print multiple cell types, and high-throughput capability.

Author contributions

Bioprinter development: Ahmed J Qureshi, Nami Okubo, Suchitra Derebail; Cell culture: Nami Okubo, Suchitra Derebail; Bioprinting test: Nami Okubo, Suchitra Derebail, Kheng L Goh, Kenny Dalgarno; Manuscript: Suchitra Derebail, Nami Okubo, Kenny Dalgarno.

Conflicts of interest

None.

Funding

This work was supported by grant funds from School of Applied Science, and Office of Technology Development, Republic Polytechnic (RP), grant number IGO (MO8)/16RIGO02 and postgraduate funds from Newcastle University in Singapore (NUIS).

Acknowledgments

The project was provided consistent technical support by Ms Fatimatuz Zahrak, Technical Support Officer at Republic Polytechnic (RP). The project was given consistent support by Mr Ashley Chua, Director of School of Applied Science (SAS,RP) and Mr Lim Boon Whatt, Director of Office of Technology Development (OTD, RP).

References

[1] R.J. Klebe, Department of Cellular and Structural Biology, U. of T. H. S. C. Cytoscribing: a method for micropositioning cells and the construction of two- and three-dimensional synthetic tissues, Exp. Cell Res. 179 (2) (1988) 362–373. https://doi.org/10.1016/0014-4827(88)90275-3.

[2] Y. Fang, R.M. Eglen, Three-dimensional cell cultures in drug discovery and development. *SLAS Discov*, Adv. Life Sci. 22 (5) (2017) 456–472. https://doi.org/10.1177/1087057117696795.

[3] H. Yurie, et al., The efficacy of a scaffold-free bio 3D conduit developed from human fibroblasts on peripheral nerve regeneration in a rat sciatic nerve model, PLoS One 12 (2017) 1–16, https://doi.org/10.1371/journal.pone.0171448.

[4] J. Yang, Y.S. Zhang, K. Yue, A. Khademhosseini, Cell-laden hydrogels for osteochondral and cartilage tissue engineering, Acta Biomater. 57 (2017) 1–25. https://doi.org/10.1016/j.actbio.2017.01.036.

[5] C. Mandrycky, Z. Wang, K. Kim, D.H. Kim, 3D bioprinting for engineering complex tissues, Biotechnol. Adv. 34 (4) (2016) 422–434, https://doi.org/10.1016/j.biotechadv.2015.12.011.

[6] G.M. Abouna, Organ shortage crisis: problems and possible solutions, Transplant. Proc. 40 (1) (2008) 34–38, https://doi.org/10.1016/j.transproceed.2007.11.067.

[7] S.V. Murphy, A. Atala, 3D bioprinting of tissues and organs, Nat. Biotechnol. 32 (8) (2014) 773–785, https://doi.org/10.1038/nbt.2958.

[8] L. Ouyang, R. Yao, Y. Zhao, W. Sun, Effect of bioink properties on printability and cell viability for 3D bioplotting of embryonic stem cells, Biofabrication 8 (3) (2016) 35020, https://doi.org/10.1088/1758-5090/8/3/035020.

[9] I.T. Ozbolat, K.K. Moncal, H. Gudapati, Evaluation of bioprinter technologies, Addit. Manuf. 13 (2017) 179–200. https://doi.org/10.1016/j.addma.2016.10.003.

[10] L.J. Pourchet, et al., Human skin 3D bioprinting using scaffold-free approach, Adv. Healthc. Mater. 6 (2017) 1–8, https://doi.org/10.1002/adhm.201601101.

[11] T. Xu, et al., Hybrid printing of mechanically and biologically improved constructs for cartilage tissue engineering applications, Biofabrication 5 (2012) 15001, stacks.iop.org/BF/5/015001.

[12] I.T. Ozbolat, Y. Yu, Bioprinting towards organ fabrication: challenges and future trends, IEEE Trans. Biomed. Eng. 60 (3) (2013) 691–699, https://doi.org/10.1109/TBME.2013.2243912.

[13] Y. Yu, et al., Three-dimensional bioprinting using self-assembling scalable scaffold-free 'tissue strands' as a new bioink, Sci. Rep. 6 (2016) 28714, https://doi.org/10.1038/srep28714.

[14] J.A. Reid, et al., Accessible bioprinting: adaptation of a low-cost 3D-printer for precise cell placement and stem cell differentiation, Biofabrication 8 (2) (2016) 25017, https://doi.org/10.1088/1758-5090/8/2/025017.

[15] T. Xu, J. Jin, C. Gregory, J.J. Hickman, T. Boland, Inkjet printing of viable mammalian cells, Biomaterials 26 (1) (2005) 93–99, https://doi.org/10.1016/j.biomaterials.2004.04.011.

[16] U. Demirci, et al., Single cell epitaxy by acoustic picolitre droplets, Lab Chip 7 (9) (2007) 1139, https://doi.org/10.1039/b704965j.

[17] H. Gudapati, M. Dey, I. Ozbolat, A comprehensive review on droplet-based bioprinting: past, present and future, Biomaterials 102 (2016) 20–42. https://doi.org/10.1016/j.biomaterials.2016.06.012.

[18] W.L. Ng, J.M. Lee, W.Y. Yeong, M. Win Naing, Microvalve-based bioprinting – process, bio-inks and applications, Biomater. Sci. 5 (4) (2017) 632–647.

[19] A. Faulkner-Jones, et al., Development of a valve-based cell printer for the formation of human embryonic stem cell spheroid aggregates, Biofabrication 5 (1) (2013) 15013, https://doi.org/10.1088/1758-5082/5/1/015013.

[20] J.A. Barron, P. Wu, H.D. Ladouceur, B.R. Ringeisen, Biological laser printing: a novel technique for creating heterogeneous 3-dimensional cell patterns, Biomed. Microdevices 6 (2) (2004) 139–147.

[21] C.J. Ferris, K.G. Gilmore, G.G. Wallace, Het Panhuis, M. Biofabrication, An overview of the approaches used for printing of living cells, Appl. Microbiol. Biotechnol. 97 (10) (2013) 4243–4258, https://doi.org/10.1007/s00253-013-4853-6.

[22] B. Guillotin, F. Guillemot, Cell patterning technologies for organotypic tissue fabrication, Trends Biotechnol. 29 (4) (2011) 183–190, https://doi.org/10.1016/j.tibtech.2010.12.008.

[23] L.D.K. Buttery, A.E. Bishop, Introduction to tissue engineering, Biomater. Artif. Organs Tissue Eng. 193–200 (2005). https://doi.org/10.1533/9781845690861.4.193.

[24] N.R. Schiele, et al., Laser-based direct-write techniques for cell printing, Biofabrication 2 (3) (2010) 32001, https://doi.org/10.1088/1758-5082/2/3/032001.

[25] R.E. Walpole, R.H. Myers, S.L. Myers, K.E. Ye, Probability and Statistics for Engineers and Scientists, ninth ed., 2011.

[26] R.E. Walpole, R.H. Myers, S.L. Myers, K.E. Ye, Probability and Statistics for Engineers and Scientists, Pearson New International Edition, *Royal Society of Chemistry* (Pearson Education Limited, 2013.

[27] L. Horváth , Engineering an in vitro air-blood barrier by 3D bioprinting, Sci. Rep. 5 (2015) 7974, https://doi.org/10.1038/srep07974.

[28] A. Faulkner-Jones, et al., Bioprinting of human pluripotent stem cells and their directed differentiation into hepatocyte-like cells for the generation of mini-livers in 3D, Biofabrication 7 (4) (2015) 44102, https://doi.org/10.1088/1758-5090/7/4/044102.

[29] W. Lee, et al., On-demand three-dimensional freeform fabrication of multi-layered hydrogel scaffold with fluidic channels, Biotechnol. Bioeng. 105 (6) (2010) 1178–1186, https://doi.org/10.1002/bit.22613.

[30] W. Zhao, X. Ji, F. Zhang, L. Li, L. Ma, Embryonic stem cell markers, Molecules 17 (6) (2012) 6196–6236, https://doi.org/10.3390/molecules17066196.

[31] J.L. Drury, D.J. Mooney, Hydrogels for tissue engineering: scaffold design variables and applications, Biomaterials 24 (2003) 4337–4351, https://doi.org/10.1016/S0142-9612(03)00340-5.

[32] V. Lee, et al., Design and fabrication of human skin by three-dimensional bioprinting, Tissue Eng. C Methods 20 (6) (2014) 473–484, https://doi.org/10.1089/ten.tec.2013.0335.

[33] S. Vijayavenkataraman, W.F. Lu, J.Y. Fuh, 3D bioprinting of skin: a state-of-the-art review on modelling, materials, and processes, Biofabrication 8 (3) (2016) 32001, https://doi.org/10.1088/1758-5090/8/3/032001.

[34] W.L. Ng, S. Wang, W.Y. Yeong, M.W. Naing, Skin bioprinting: impending reality or fantasy? Trends Biotechnol. 34 (9) (2016) 689–699. https://doi.org/10.1016/j.tibtech.2016.04.006.

[35] D. Abbey, P.B. Seshagiri, Ascorbic acid-mediated enhanced cardiomyocyte differentiation of mouse ES-cells involves interplay of DNA methylation and multiple-signals, Differentiation 96 (2017) 1–14. https://doi.org/10.1016/j.diff.2017.04.001.

[36] X. Shen, et al., Differentiation of mesenchymal stem cells into cardiomyocytes is regulated by miRNA-1-2 via WNT signaling pathway, J. Biomed. Sci. 24 (1) (2017) 1–8, https://doi.org/10.1186/s12929-017-0337-9.

[37] A. Trenti, et al., Therapeutic Concentrations of Digitoxin Inhibit Endothelial Focal Adhesion Kinase and Angiogenesis Induced by Different Growth Factors, 2017, 174 (18) 3094–3016, https://doi.org/10.1111/bph.13944.